Hindawi
Advances in Condensed Matter Physics
Volume 2023, Article ID 6463744, 11 pages
https://doi.org/10.1155/2023/6463744

Research Article

Gate Voltage-Modulated Conductance in Zigzag Graphene Nanoribbon Junctions

Ming Li, Zhi-Bo Feng, and Zheng-Yin Zhao

School of Science, Xuchang University, Xuchang 461000, China

Correspondence should be addressed to Ming Li; mingli245@163.com

Received 18 February 2023; Revised 15 April 2023; Accepted 28 July 2023; Published 25 August 2023

Academic Editor: Shobhit K. Patel

Using the Green's function method, we study the modulation of the conductance in zigzag graphene nanoribbon (ZGNR) junctions by the gate voltages. As long as the difference between the gate voltages applied on the left and right ZGNRs (ΔV) remains unchanged, the conductance profiles for different cases are exactly the same, except to a displacement along E_F-axis. It is found that the transmission of electrons from the upper/lower edge state of the left ZGNR to the lower/upper edge state of the right ZGNR is forbidden, therefore, the width of the conductance gap increases first and then decreases as $|\Delta V|$ increases. The upper/lower edge states and conduction/valence subbands of ZGNR under higher/lower gate voltage (V_H/V_L) determine step positions of the conductance when $E_F > V_H/E_F < V_L$. But when $V_L \leq E_F \leq V_H$, the conductance profile is mainly determined by the upper and lower edge states, a few lowest conduction subbands/topmost valence subbands of ZGNR under lower/higher gate voltage. These results are helpful to the exploration and application of a new kind of field effect transistor based on ZGNR junctions.

1. Introduction

Graphene has excellent electrical, optical, and thermal properties, and has been considered as a perspective base for the postsilicon electronics since the successful fabrication in experiment [1–4]. Around the Dirac points, the band structure of graphene presents a linear dispersion, and the quasiparticles obey the massless Dirac equation and relativistic-like behaviors appear [3–7]. If graphene is patterned into graphene nanoribbon (GNR), interesting properties emerge [8]. For example, the edge states are found in graphene nanostructures with zigzag edge [4, 9–15]. In fact, many interesting phenomena in graphene and other novel two dimensional honeycomb lattice materials are in nature associated with the edge states [4, 9, 15–20], e.g., the valley-filtered transport [10, 21–23] and magnetism [11–13].

Furthermore, by interconnecting two semi-infinite GNRs with different widths, a GNR junction can be obtained [17, 23]. The conductance of metal–semiconductor GNR junctions, which is the key elements in all-graphene circuits, has attracted extensive research recently [24–26]. Due to the mismatch between conducting channels in the left and right GNRs, a traveling carrier is strongly scattered at the junction interface and a finite junction conductance is induced [17, 23, 27, 28]. Therefore, the junction conductance strongly depends on the geometry of the junction interface [24].

Experimentally, the Fermi level (E_F) in the GNR can be above or below the Dirac points by tuning the gate voltage, then the global or local charge carriers can be easily tuned from electron like to hole like and vice versa [1, 4, 5, 29, 30]. Moreover, the transport of topological edge states can be manipulated by adjusting the gate voltage embedding on the surface of two-dimensional topological insulator systems [31], and the spin polarization [32], spin inversion [33], and valley polarization [34] in silicene nanoribbons can also be manipulated by the gate voltage.

However, to the best of our knowledge, modulation of the electronic and transport properties of zigzag graphene nanoribbon (ZGNR) junctions by the gate voltages applied on the left and right ZGNRs (V_{gL} and V_{gR}, with $\Delta V = V_{gL} - V_{gR}$) has not been studied, which is crucial for designing all-graphene junctions and circuits [35]. Thus in this paper, to explore how the gate voltage affects the conductance channels (the edge states, the conduction, and valence subbands) and the mode matching between the left and right ZGNRs, we study how the

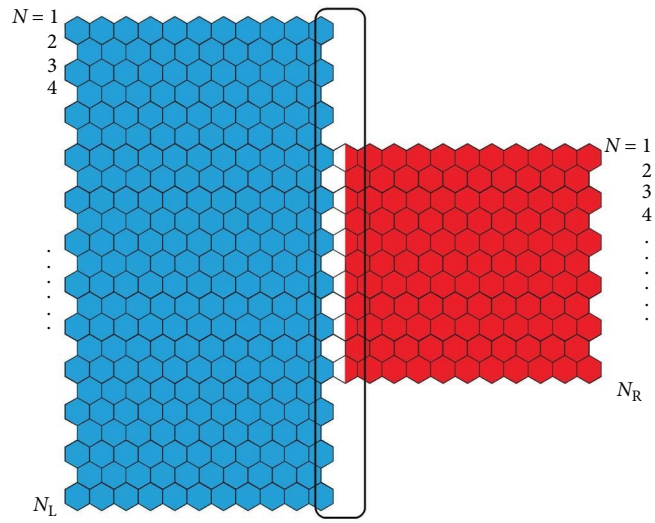

FIGURE 1: Geometry of the ZGNR junction. The blue (red) region denotes the left (right) ZGNR on which the gate voltage V_{gL} (V_{gR}) is applied. The interface between the two semi-infinite GNRs that form the junction is marked with a black box, which is chosen as the central conduction region.

conductance of the ZGNR junction depends on the gate voltage applied on the left and right ZGNRs. The G–E_F curves in all cases can be clarified from the energy band structures of the left and right ZGNRs. For $V_{gL} = 0$ ($V_{gR} = 0$), the G profiles for opposite V_{gR} (V_{gL}) are symmetric to each other with respect to $E_F = 0$, and they move further away from each other with increasing $|\Delta V|$. For a given ΔV, the G profiles for different V_{gL} or V_{gR} are identical, except to a displacement along E_F-axis. The transmission probability of electrons from the upper/lower edge state of the left ZGNR to the lower/upper edge state of the right ZGNR is found to be 0. As a result, the width of the conductance gap increases first and then decreases with increasing $|\Delta V|$.

The rest of the paper is organized as follows. In Section 2, the Green's function method, the tight-binding model, and the geometrical structure of the ZGNR junction are introduced in brief. In Section 3, the dependance of the conductance of the ZGNR junction on the gate voltages applied on the left and right ZGNRs is studied and analyzed in detail. Finally, conclusions are given in Section 4.

2. Theory and Model

Figure 1 shows the geometry of the zigzag ZGNR junction connecting the left and right leads (semi-infinite ZGNR). From the top to down, atoms in a unit cell are labeled as 1, 2, …, N_L/N_R. Here N_L/N_R denotes the width of the left/right ZGNR.

The Hamiltonian for the ZGNR junction reads [5, 36–39]

$$H = -t \sum_{<ij>\alpha} c_{i\alpha}^{+} c_{j\alpha} + V_g \sum_{i\alpha} c_{i\alpha}^{+} c_{i\alpha}. \quad (1)$$

Here $t = 2.75$ eV is the transfer energy of the nearest neighbor hopping, $<ij>$ represents the nearest neighbors, α denotes the spin index, and E_F is the gate voltage applied on the ZGNR.

The conductance of the ZGNR junction can be calculated from the Landauer–Büttiker formula [40, 41],

$$G(E) = G_0 \mathrm{Tr}[\Gamma_L G^r \Gamma_R G^a]. \quad (2)$$

Here $G_0 = 2e^2/h$ is the unit quanta of conductance considering the spin degeneracy [26]. $G^r = [G^a]^+ = [E - H_{\mathrm{cen}} - \sum_L^r - \sum_R^r]^{-1}$ is the retarded Green function [42, 43]. $\sum_{L,R}^r = H_{01}^+ g_{L,R} H_{01}$ is the self-energy, $\Gamma_{L,R}^r = i[\sum_{L,R}^r - (\sum_{L,R}^r)^+]$ is the line width function, and $g_{L/R}$ is the surface Green function of the left/right semi-infinite ZGNR [44–47].

3. Results and Discussion

In this section, assuming $N_L = 40$ and $N_R = 20$, the dependance of the conductance of the ZGNR junction on the gate voltages applied on the left and right ZGNRs is studied and analyzed in detail. The G–E_F curves are clearly clarified by analyzing the energy band structures of the left and right ZGNRs. First, the conductance of the ZGNR junction for $V_{gR} = 0$ and different V_{gL} are explored. Second, for $V_{gL} = 0$, how G depends on V_{gR} is analyzed. Next, assuming $V_{gL} = -V_{gR} = V_g$, the variation of G as a function of V_g is considered. Finally, for a given ΔV, the G profiles of the ZGNR junction under different V_{gL} or V_{gR} are compared.

3.1. Conductance of the ZGNR Junction for $V_{gR} = 0$ and Different V_{gL}. In Figures 2(a)–2(d) and 3(a)–3(d), we show G versus E_F in the ZGNR junction for $V_{gR} = 0$ and $V_{gL} = 0$, 0.018, ±0.4, ±0.8, 0.8964, and 1.2 eV, and the corresponding energy band structures of ZGNRs.

When $V_{gR} = 0$, the G profile for $V_{gL} = V_g$ is symmetric to that for $V_{gL} = -V_g$ with respect to $E_F = 0$, i.e., $G(E_F)|_{V_{gL}=V_g} = G(-E_F)|_{V_{gL}=-V_g}$, because the conduction and valecne subbands

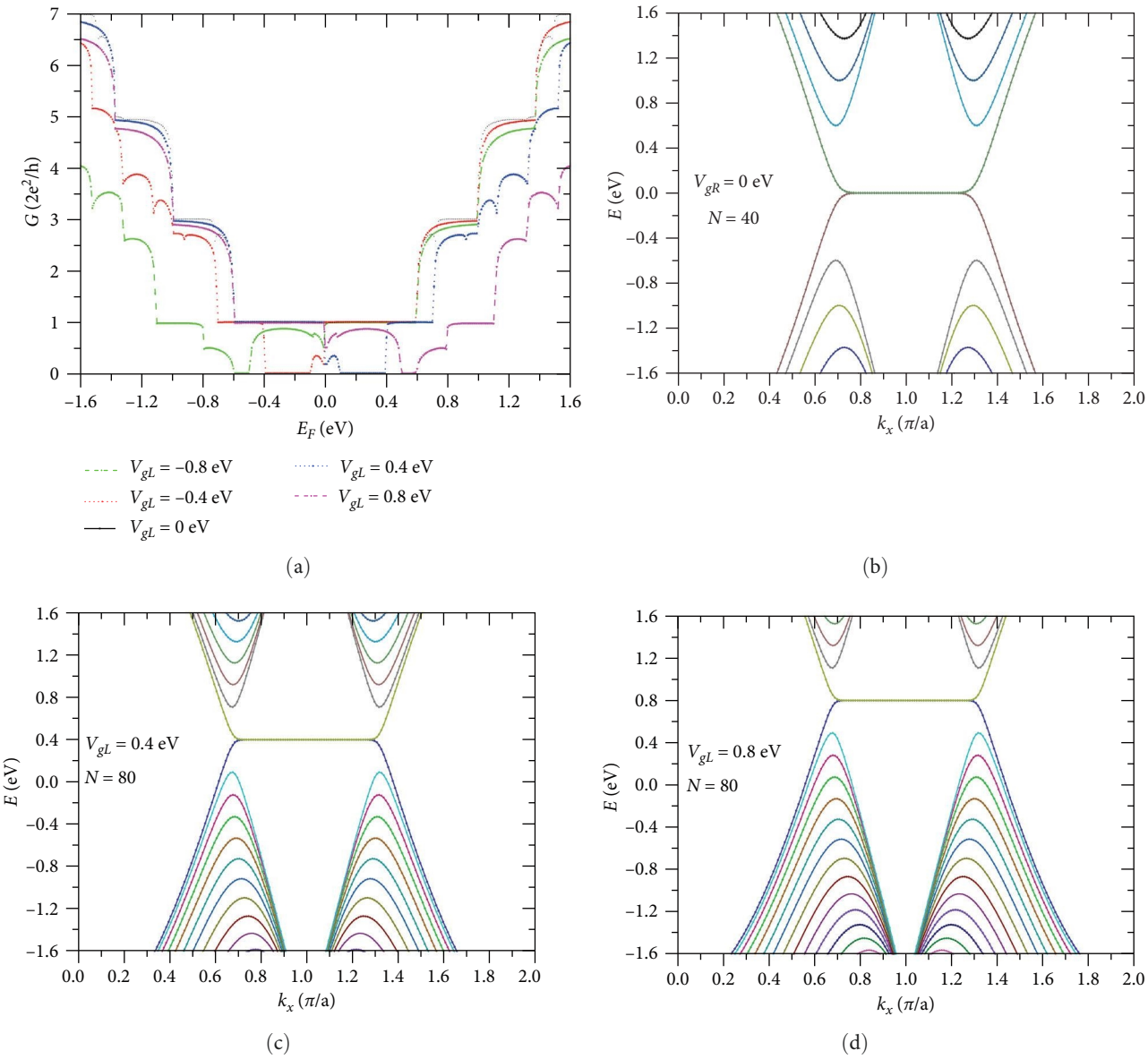

FIGURE 2: G versus E_F in the ZGNR junction for $V_{gR}=0$ and $V_{gL}=0$, ± 0.4, and ± 0.8 eV, and the corresponding energy band structures of ZGNRs (a, b, c, d).

are just reversed when the sign of the gate voltage applied on the left ZGNR is reversed. With the increase of $|V_{gL}|$, the profile of $G(E_F)|_{V_{gL}=V_g}$ moves further away from that of $G(E_F)|_{V_{gL}=-V_g}$, and G decreases as a whole, because the energy mismatch of the conducting channels increases.

For $V_{gL}>0$ ($V_{gL}<0$) and $E_F>V_{gL}$ ($E_F<V_{gL}$), G decreases with the increase of $|V_{gL}|$ as a whole, and step positions of G are determined by the upper (lower) edge state and conduction (valence) subbands of ZGNR under higher (lower) gate voltage. For $V_{gL}>0$ ($V_{gL}<0$) and $E_F<0$ ($E_F>0$), G for different V_{gL} are in proximity to that of $V_{gL}=0$, especially for a lower $|E_F|$, since step positions of G are mainly determined by the lower (upper) edge states and the valence (conduction) subbands of ZGNR under lower (higher) gate voltage. When $V_{gL}=V_{gR}$, step positions of G are just decided by the subbands of the right narrower ZGNR.

When $0.018 \le |V_{gL}| \le 0.8964$ eV and $V_{gL}>0$ ($V_{gL}<0$), there is a conductance gap at the positive (negative) direction of E_F-axis. By increasing $|V_{gL}|$, the width of the conductance gap increases first and then decreases. These originate from that the transmission of electrons from the upper/lower edge state of the left ZGNR to the lower/upper edge state of the right ZGNR is forbidden. In fact, when the zigzag-chain number N is even (here $N_L=40$ and $N_R=20$), the electron transport in the ZGNR should satisfy the pseudoparity conservation and the valley valve effect appears [10, 46, 48], so electrons of the lower/upper edge state in the left ZGNR cannot transmit to the upper/lower edge sate in the right ZGNR.

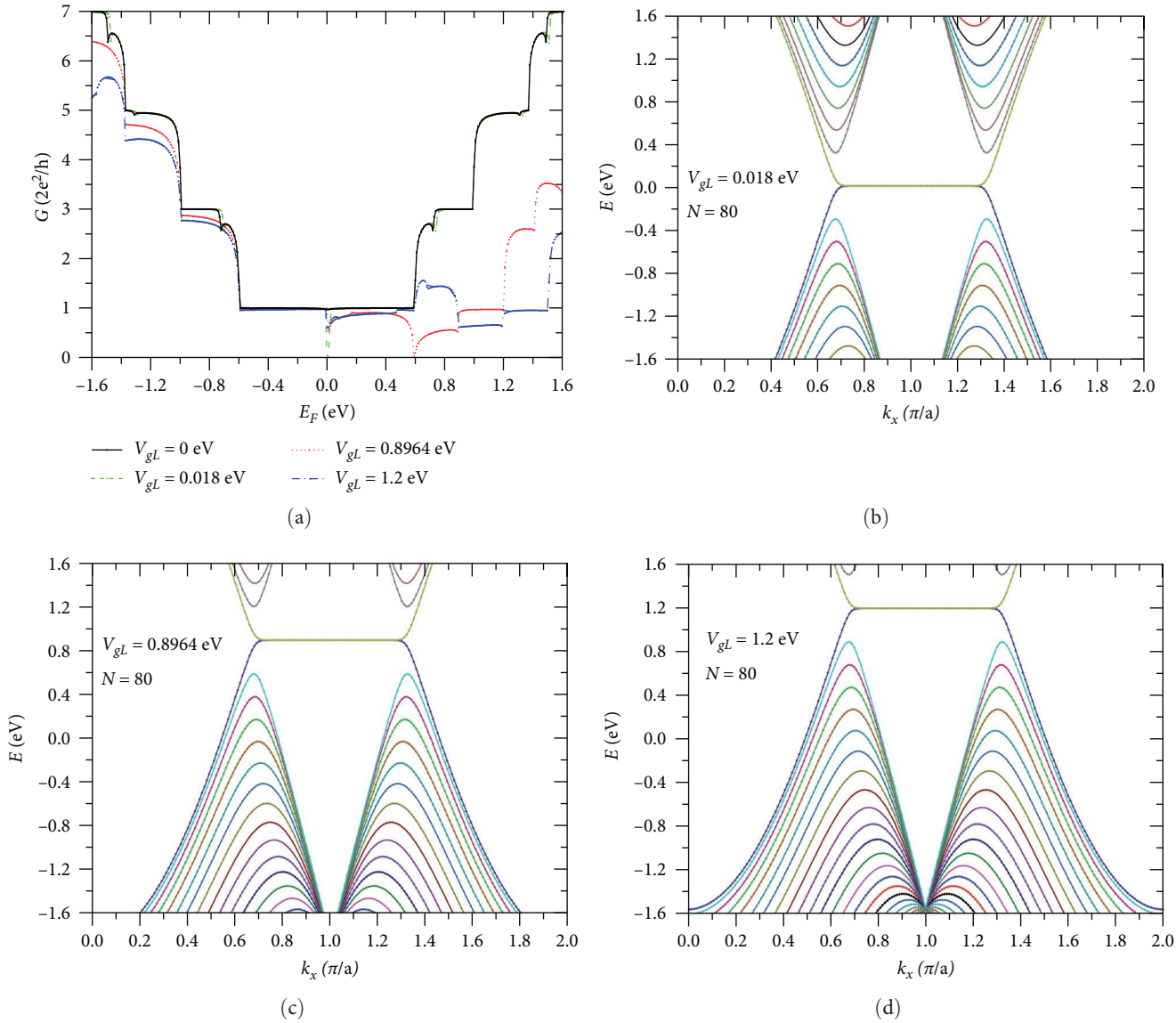

FIGURE 3: G versus E_F in the ZGNR junction for $V_{gR} = 0$ and $V_{gL} = 0$, 0.018, 0.8964, and 1.2 eV, and the corresponding energy band structures of ZGNRs (a, b, c, and d).

When $V_{gL} = 0.018$ eV, the profile of G is almost the same as that of $V_{gL} = 0$, but G decreases abruptly to 0 at $E_F = 0.018$ eV, then increases rapidly to a $1 \cdot G_0$ plateau at $E_F = 0$ eV. With further increasing V_{gL}, the conduction gap begins to form and the width of conduction gap increases. This is determined by the lower edge state of ZGNR under higher gate voltage and lower edge state of ZGNR under lower gate voltage.

When $V_{gL} = 0.4$ eV, with the decrease of E_F, G decreases to a $1 \cdot G_0$ plateau at $E_F = 0.7$ eV, and decreases to a 0 plateau at $E_F = 0.4$ eV, which is determined by the conduction subbands and the upper and lower edge states of ZGNR under higher gate voltage. Then G increases to a $0.5 \cdot G_0$ plateau at $E_F = 0.1$ eV, which is determined by the topmost valence subband of ZGNR under higher gate voltage. So the conductance gap is in the E_F interval [0.1, 0.4 eV], rather than [0, 0.4 eV], which is determined by the topmost valence subband and lower edge state of ZGNR under higher gate voltage. Finally, G shows a dip at $E_F = 0$ and increases step by step as E_F decreases, which is determined by the lower edge state and valence subbands of ZGNR under lower gate voltage.

When $V_{gL} = 0.8$ eV, with the decrease of E_F, G decreases to a $0.5 \cdot G_0$ plateau at $E_F = 0.8$ eV. Then G decreases to a 0 plateau at $E_F = 0.59$ eV, and increases to a $0.8 \cdot G_0$ plateau at $E_F = 0.5$ eV, which is determined by the lowest conduction subband of ZGNR under lower gate voltage and topmost valence subband of ZGNR under higher gate voltage. So the conductance gap is in the E_F interval [0.5, 0.59 eV], rather than [0, 0.8 eV].

When $V_{gL} = 0.8964$ eV, the edge position of the lowest conduction subband of ZGNR under lower gate voltage just coincides with that of the topmost valence subband of ZGNR under higher gate voltage, so G decreases to 0 and increases

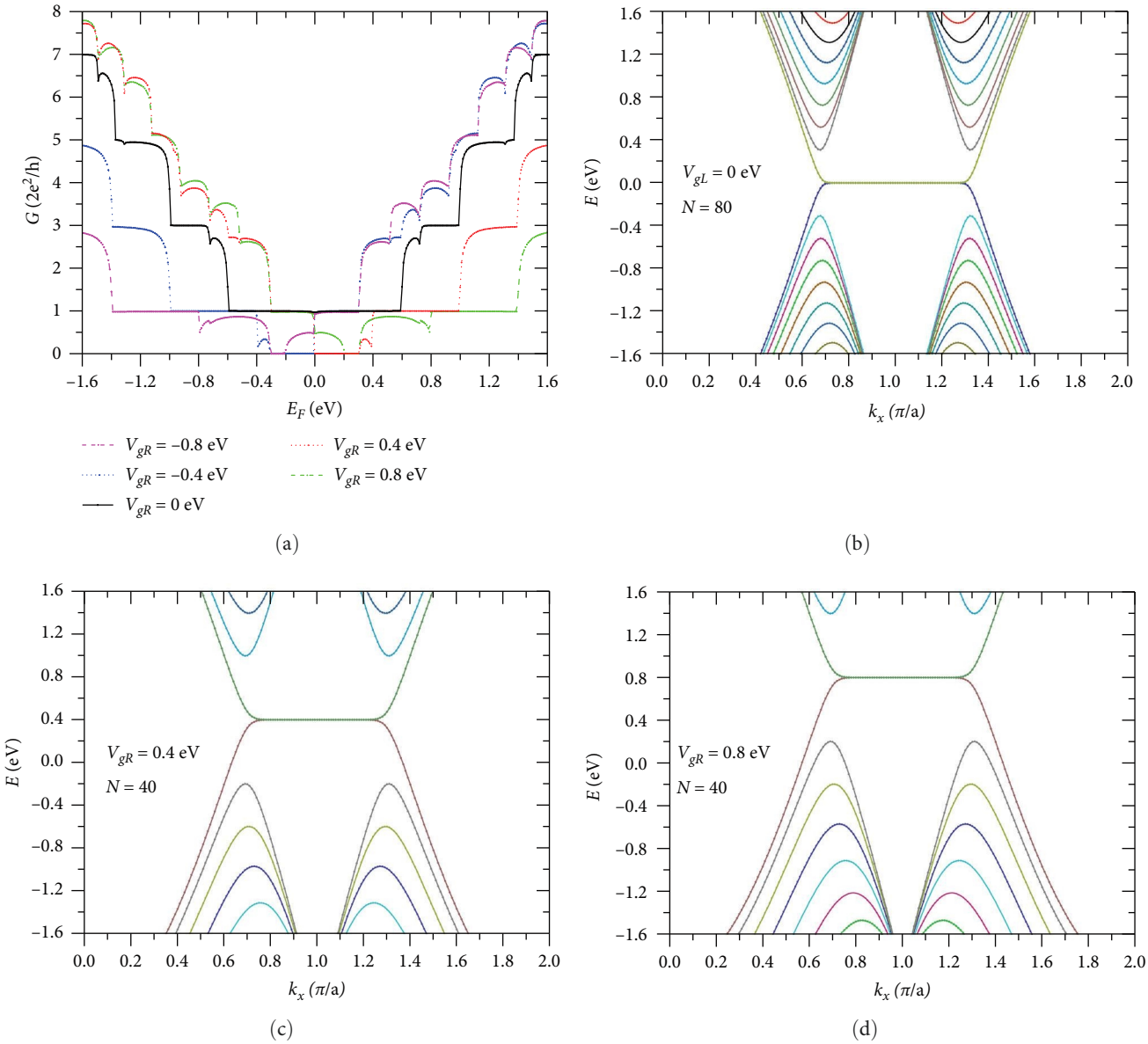

FIGURE 4: G versus E_F in the ZGNR junction for $V_{gL} = 0$ and $V_{gR} = 0$, ± 0.4, and ± 0.8 eV, and the corresponding energy band structures of ZGNRs (a, b, c, and d).

rapidly to a $0.8 \cdot G_0$ plateau at $E_F = 0.59$ eV with the decrease of E_F. Therefore, the conduction gap begins to disappear, rather than lies in the E_F interval [0, 0.8964 eV]. With further increasing V_{gL}, there is no conduction gap.

When $V_{gL} = 1.2$ eV, with the decrease of E_F, G increases to a $1.4 \cdot G_0$ plateau at $E_F = 0.91$ eV, and decreases to a $0.9 \cdot G_0$ plateau at $E_F = 0.59$ eV. This is also determined by the topmost valence subband of ZGNR under higher gate voltage and the lowest conduction subband of ZGNR under lower gate voltage.

3.2. Conductance of the ZGNR Junction for $V_{gL} = 0$ and Different V_{gR}. In Figures 4(a)–4(d) and 5(a)–5(d), we show G versus E_F in the ZGNR junction for $V_{gL} = 0$ and $V_{gR} = 0$, 0.018, ± 0.4, ± 0.8, 0.8964, and 1.2 eV, and the corresponding energy band structures of ZGNRs.

Here the G profiles for $V_{gL} = 0$ and different V_{gR} can be discussed similarly as that in Section 3.1 for $V_{gR} = 0$ and different V_{gL}, and the G profiles are found to be the same. For example, the G profiles for $V_{gR} = 0$ and $V_{gL} = -0.8$, -0.4, 0.4, and 0.8 shown in Figure 2(a) are the same to that for $V_{gL} = 0$ and $V_{gR} = 0.8$, 0.4, -0.4, and -0.8 shown in Figure 4(a), respectively. By comparing the G profiles for the above cases, it is found that as long as the difference between the gate voltages applied on the left and right ZGNRs (ΔV) remains unchanged, the conductance profiles for different cases are exactly the same, except to a displacement along E_F-axis. This general rule and detailed reasons will be further discussed in Section 3.4.

3.3. Conductance of the ZGNR Junction for $V_{gL} = -V_{gR}$. Figure 6 shows G versus E_F in the ZGNR junction for $V_{gL} =$

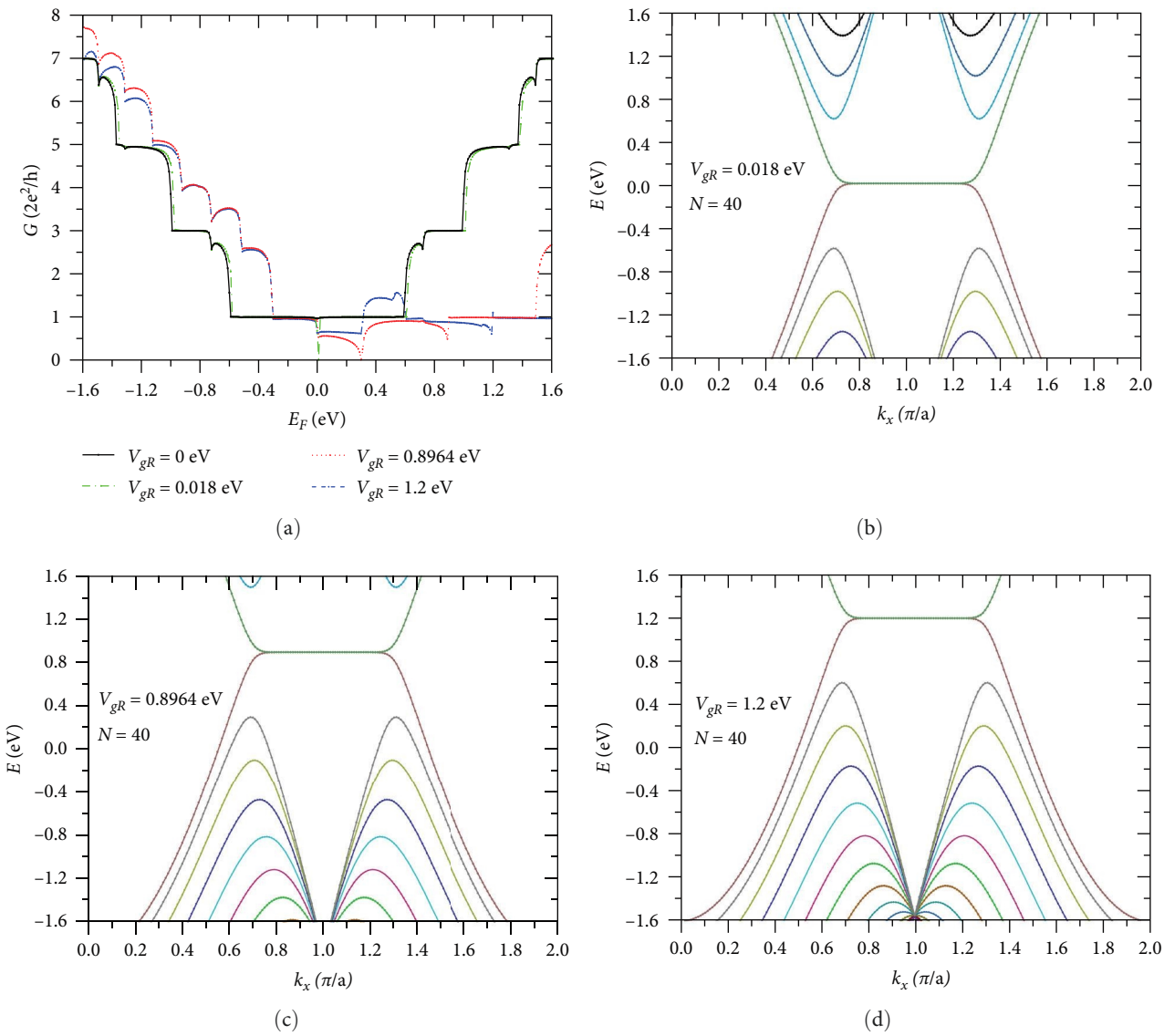

FIGURE 5: G versus E_F in the ZGNR junction for $V_{gL}=0$ and $V_{gR}=0$, 0.018, 0.8964, and 1.2 eV, and the corresponding energy band structures of ZGNRs (a, b, c, and d).

$-V_{gR}=V_g=0.009$, ± 0.4, 0.4482, and 0.8 eV and Figures 7 (a1–a4) and 7(b1–b4) show the corresponding energy band structures of ZGNRs.

The G profile for $V_{gL}=-V_{gR}=V_g$ is symmetric to that for $V_{gL}=-V_{gR}=-V_g$ with respect to $E_F=0$, i.e., $G(E_F)|_{V_{gL}=-V_{gR}=V_g}=G(-E_F)|_{V_{gL}=-V_{gR}=-V_g}$, because the conduction and valence subbands are just reversed when the sign of the gate voltage applied on the left/right ZGNR is reversed. With the increase of $|V_g|$, the profile of $G(E_F)|_{V_{gL}=-V_{gR}=V_g}$ moves further away from that of $G(E_F)|_{V_{gL}=-V_{gR}=-V_g}$, and G decreases as a whole, because the energy mismatch of the conducting channels increases.

For $V_g>0$ ($V_g<0$) and $E_F>V_g$ ($E_F<V_g$), step positions of G are determined by the upper (lower) edge states and conduction (valence) subbands of ZGNR under higher (lower) gate voltage. For $V_g>0$ ($V_g<0$) and $E_F<-V_g$ ($E_F>-V_g$), step positions of G are mainly determined by the lower (upper) edge states and the valence (conduction) subbands of ZGNR under lower (higher) gate voltage.

When $0.009\leq|V_g|\leq 0.4482$ eV and $V_g>0$ ($V_g<0$), there is a conductance gap at the positive (negative) direction of E_F-axis. With the increase of $|V_g|$, the width of the conductance gap first increases and then decreases. As discussed above, these originate from that the transmission of electrons from the upper/lower edge state of the left ZGNR to the lower/upper edge state of the right ZGNR is forbidden as a result of the pseudoparity conservation and the valley valve effect [10, 46, 48]. Here the G profiles are the same to that for $0.018\leq|V_{gL}|\leq 0.8964$ eV and $V_{gR}=0$, because ΔV in the above two cases is the same.

When $V_g=0.009$ eV, the profile of G is almost the same as that of $V_g=0$, but G decreases abruptly to 0 around $E_F=0.009$ eV, then increases rapidly to a $1\cdot G_0$ plateau at $E_F=-0.009$ eV, namely, the $1\cdot G_0$ plateau shows a conductance dip to

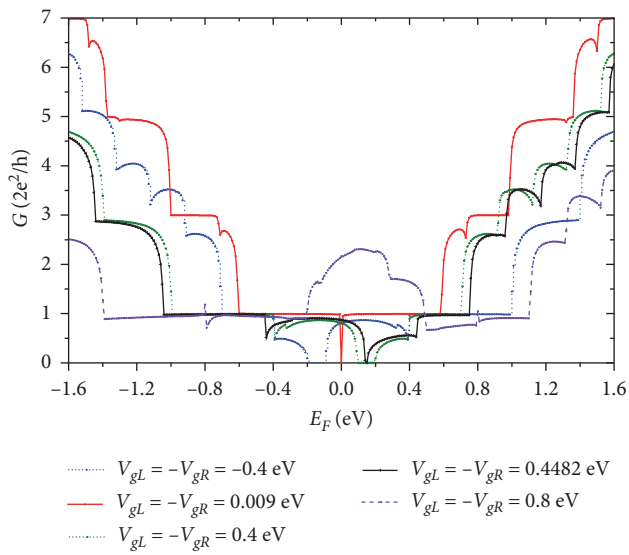

FIGURE 6: G versus E_F in the ZGNR junction for $V_{gL} = -V_{gR} = V_g = 0.009$, ± 0.4, 0.4482, and 0.8 eV.

0 at $E_F = 0$. With further increasing V_g, the conduction gap begins to form and the width of conduction gap increases. This is determined by the lower edge state of ZGNR under higher gate voltage and upper edge state of ZGNR under lower gate voltage. Here the G profiles are the same to that for $V_{gL} = 0.18$ eV and $V_{gR} = 0$, because ΔV in the above two cases is the same.

When $V_g = 0.4$ eV, with the decrease of E_F, G decreases to a $1 \cdot G_0$ plateau at $E_F = 0.7$ eV, and decreases to a $0.5 \cdot G_0$ plateau at $E_F = 0.4$ eV, which is determined by the conduction subbands and the upper and lower edge states of ZGNR under higher gate voltage. Then G decreases slowly to a 0 plateau at $E_F = 0.2$ eV, and increases to a $0.8 \cdot G_0$ plateau at $E_F = 0.1$ eV, which is determined by the lowest conduction subband of ZGNR under lower gate voltage and the topmost valence subband of ZGNR under higher gate voltage. So the conductance gap is in the E_F interval [0.1, 0.2 eV], rather than [0, 0.4 eV]. Finally, G shows a dip and increases to a $1 \cdot G_0$ plateau at $E_F = -0.4$ eV, then increases step by step with the decrease of E_F. This is determined by the upper and lower edge states and valence subbands of ZGNR under lower gate voltage. Here the G profiles are the same to that for $V_{gL} = 0.8$ eV and $V_{gR} = 0$, because ΔV in the above two cases is the same.

When $V_g = 0.4482$ eV, the edge position of the lowest conduction subband of ZGNR under lower gate voltage just coincides with that of the topmost valence subband of ZGNR under higher gate voltage, so G decreases to 0 and increases rapidly to a $0.9 \cdot G_0$ plateau at $E_F = 0.15$ eV with the decrease of E_F. Therefore, the conduction gap begins to disappear, rather than lies in the E_F interval [0, 0.4482 eV]. As $|V_g|$ increases, there is no conduction gap. Here the G profiles are the same to that for $V_{gL} = 0.8964$ eV and $V_{gR} = 0$, because ΔV in the above two cases is the same.

When $V_g = 0.8$ eV, with the decrease of E_F, G increases to a $1.5 \cdot G_0$ plateau at $E_F = 0.48$ eV, and increases to a $2.25 \cdot G_0$ plateau at $E_F = 0.27$ eV. This is determined by the topmost two valence subbands of ZGNR under higher gate voltage. When $-0.233 \leq E_F \leq 0.27$ eV, G is determined by the upper edge state, a few lowest conduction subbands of ZGNR under lower gate voltage and a few topmost valence subbands of ZGNR under higher gate voltage. Finally, G decreases to a $0.9 \cdot G_0$ plateau at $E_F = -0.233$ eV, which is determined by the lowest conduction subband of ZGNR under lower gate voltage.

3.4. Conductance of the ZGNR Junction for $V_{gL} - V_{gR} = \Delta V$ ($G(E_F)|_{V_{gL}-V_{gR}=\Delta V}$). In this Section 3.4, the G profiles of the ZGNR junction for the same ΔV but different V_{gL} or V_{gR} are compared. Taking $\Delta V = 0.8$ eV as an example, the G profiles of the ZGNR junction for different V_{gL} or V_{gR} are demonstrated in Figure 8. The G profiles for the same ΔV are exactly the same, i.e., $G(E_F)|_{VgL} = G\left(E_F - V_g\right)|_{V_{gL}-V_g}$ for any V_g. If $V_g > 0$ ($V_g < 0$), the G profile for V_{gL} can be obtained by translating that for $V_{gL} - V_g$ by $|V_g|$ along the positive (negative) direction of E_F-axis. In fact, the gate voltage applied on the ZGNR will shift the position of the energy subbands (conducting channels), the transmission coefficient of electrons or holes from one channel in the left ZGNR to that of the right one is just determined by the relative positions of the above conducting channels.

Therefore, as long as the difference between the gate voltages applied on the left and right ZGNRs (ΔV) remains unchanged, the conductance profiles for different cases are exactly the same, except to a displacement along E_F-axis. Moreover, as discussed above, the width of the conductance gap increases first and then decreases as $|\Delta V|$ increases.

These results are helpful to the exploration and application of a new kind of field effect transistor (FET) based on ZGNR junctions, in which the conducting channels involved in the transmission of electrons or holes are controlled by the gate voltage, and their functions are similar to those of semiconductor FETs.

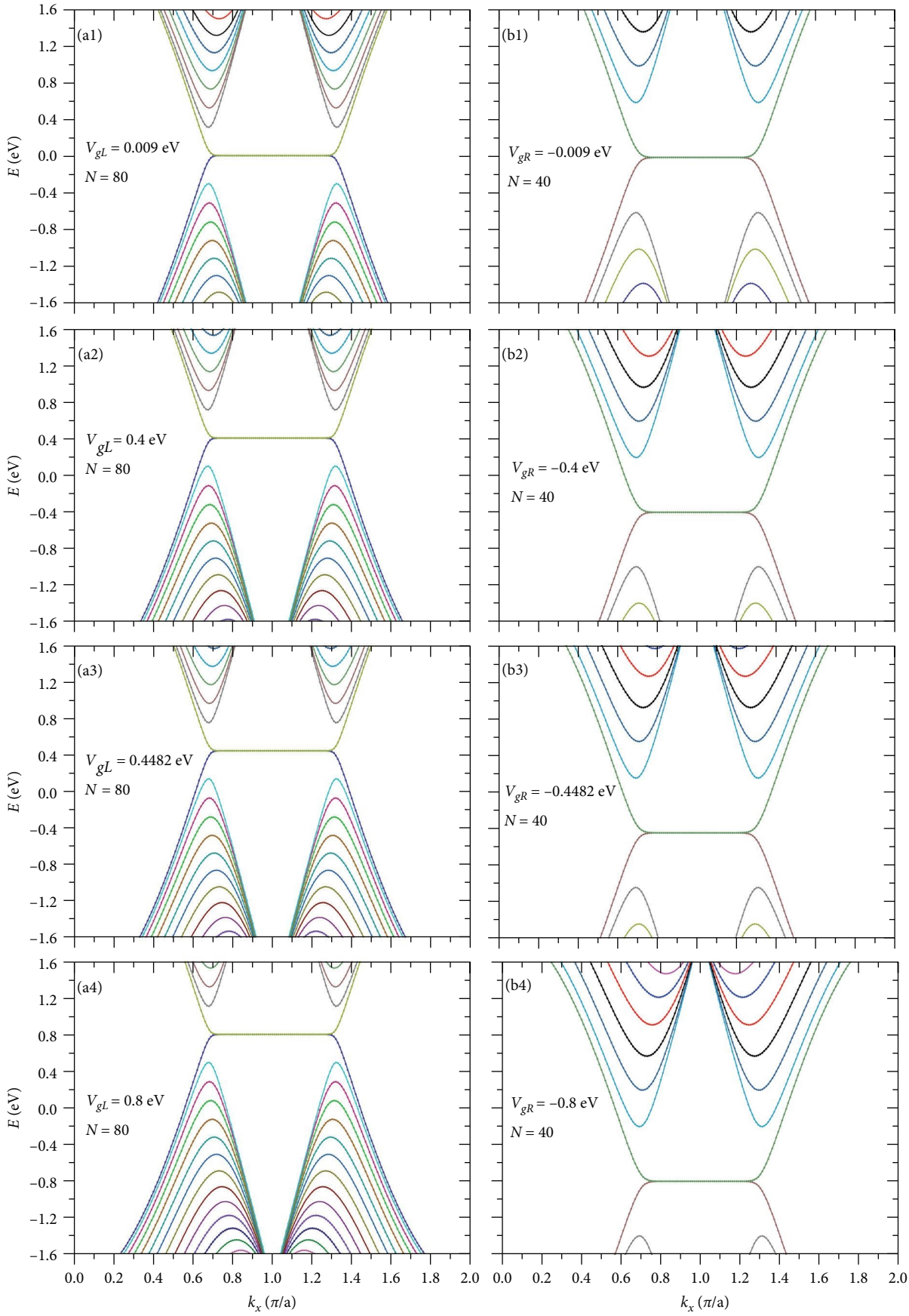

Figure 7: The energy band structures of the (a1, a2, a3, and a4) left and (b1, b2, b3, and b4) right ZGNRs under opposite gate voltages.

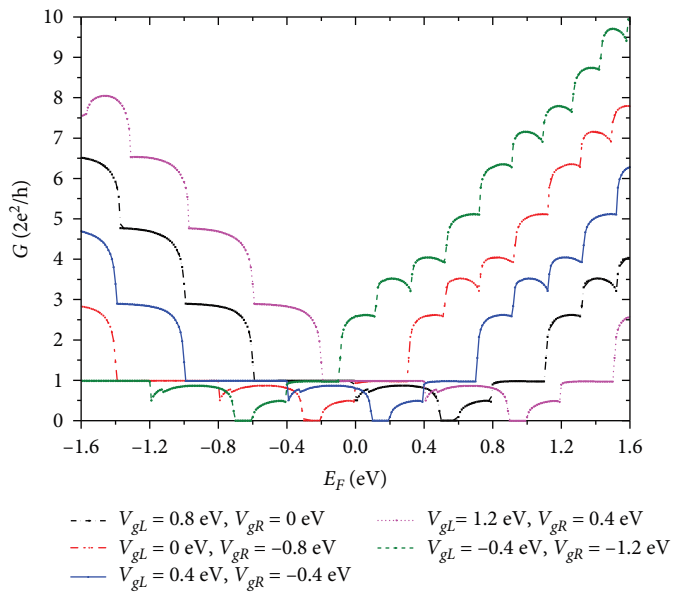

FIGURE 8: G versus E_F in the ZGNR junction for $\Delta V = 0.8$ eV but different V_{gL} or V_{gR}.

4. Conclusion

In summary, by adjusting the gate voltages applied on the left and right ZGNRs, the conductance of the ZGNR junction is studied. The G–E_F curves for all cases can be clarified from the energy band structures of the left and right ZGNRs. When $V_{gL} = 0$ ($V_{gR} = 0$), the G profiles for opposite V_{gR} (V_{gL}) are symmetric to each other with respect to $E_F = 0$, and they move further away from each other with the increase of $|\Delta V|$. For a given ΔV, the G profiles for different V_{gL} or V_{gR} are exactly the same, except to a displacement along the positive or negative direction of E_F-axis. Because the transmission of electrons from the upper/lower edge state of the left ZGNR to the lower/upper edge state of the right ZGNR is not allowed, the width of the conductance gap increases first and then decreases as $|\Delta V|$ increases. The width of the conduction gap is mainly determined by the upper and lower edge states, a few lowest conduction subbands of ZGNR under lower gate voltage and a few topmost valence subbands of ZGNR under higher gate voltage. Step positions of G are determined by the upper edge state and conduction subbands of ZGNR under higher gate voltage (E_F) when $E_F > V_{\mathrm{H}}$, and by the lower edge state and the valence subbands of ZGNR under lower gate voltage (V_{L}) when $E_F < V_{\mathrm{L}}$. These results are helpful to the exploration and application of graphene-based FETs.

Data Availability

The datasets used and/or analyzed during the current study are available from the corresponding author on reasonable request.

Conflicts of Interest

The authors declare that they have no conflicts of interest.

Acknowledgments

This work was supported by the Scientific Research Innovation Team of the Xuchang University (grant no. 2022CXTD005) and the "316" Project Plan of the Xuchang University.

References

[1] K. S. Novoselov, A. K. Geim, S. V. Morozov et al., "Electric field effect in atomically thin carbon films," *Science*, vol. 306, no. 5696, pp. 666–669, 2004.

[2] K. S. Novoselov, A. K. Geim, S. V. Morozov et al., "Two-dimensional gas of massless Dirac fermions in graphene," *Nature*, vol. 438, pp. 197–200, 2005.

[3] Y. Xing, J. Wang, and Q.-F. Sun, "Focusing of electron flow in a bipolar graphene ribbon with different chiralities," *Physical Review B*, vol. 81, Article ID 165425, 2010.

[4] Y. Xing, Q.-F. Sun, and J. Wang, "Nernst and Seebeck effects in a graphene nanoribbon," *Physical Review B*, vol. 80, no. 23, Article ID 235411, 2009.

[5] W. Long, Q.-F. Sun, and J. Wang, "Disorder-induced enhancement of transport through graphene p–n junctions," *Physical Review Letters*, vol. 101, no. 16, Article ID 166806, 2008.

[6] J. C. Slonczewski and P. R. Weiss, "Band structure of graphite," *Physical Review*, vol. 109, no. 2, pp. 272–279, 1958.

[7] A. H. Castro Neto, F. Guinea, N. M. R. Peres, K. S. Novoselov, and A. K. Geim, "The electronic properties of graphene," *Reviews of Modern Physics*, vol. 81, no. 1, pp. 109–162, 2009.

[8] A. Saffarzadeh and M. Ghorbani Asl, "Spin currents and magnetoresistance of graphene-based magnetic junctions," *The European Physical Journal B*, vol. 67, pp. 239–244, 2009.

[9] K. Nakada, M. Fujita, G. Dresselhaus, and M. S. Dresselhaus, "Edge state in graphene ribbons: nanometer size effect and edge shape dependence," *Physical Review B*, vol. 54, no. 24, pp. 17954–17961, 1996.

[10] A. Rycerz, J. Tworzydło, and C. W. J. Beenakker, "Valley filter and valley valve in graphene," *Nature Physics*, vol. 3, pp. 172–175, 2007.

[11] J. Fernández-Rossier and J. J. Palacios, "Magnetism in graphene nanoislands," *Physical Review Letters*, vol. 99, no. 17, Article ID 177204, 2007.

[12] L. Pisani, J. A. Chan, B. Montanari, and N. M. Harrison, "Electronic structure and magnetic properties of graphitic ribbons," *Physical Review B*, vol. 75, no. 6, Article ID 064418, 2007.

[13] O. Hod, V. Barone, and G. E. Scuseria, "Half-metallic graphene nanodots: a comprehensive first-principles theoretical study," *Physical Review B*, vol. 77, no. 3, Article ID 035411, 2008.

[14] C. Wang, Y. Zou, J. Song, and Y.-X. Li, "Andreev reflection in a Y-shaped graphene–superconductor device," *Physical Review B*, vol. 98, no. 3, Article ID 035403, 2018.

[15] Z. Z. Zhang, Z. H. Wu, K. Chang, and F. M. Peeters, "Resonant tunneling through S- and U-shaped graphene nanoribbons," *Nanotechnology*, vol. 20, no. 41, Article ID 415203, 2009.

[16] L. Jiang, Y. Zheng, C. Yi, H. Li, and T. Lü, "Analytical study of edge states in a semi-infinite graphene nanoribbon," *Physical Review B*, vol. 80, no. 15, Article ID 155454, 2009.

[17] H. Li, L. Wang, and Y. Zheng, "Suppressed conductance in a metallic graphene nanojunction," *Journal of Applied Physics*, vol. 105, no. 1, Article ID 013703, 2009.

[18] S.-G. Cheng, J. Zhou, H. Jiang, and Q.-F. Sun, "The valley filter efficiency of monolayer graphene and bilayer graphene line defect model," *New Journal of Physics*, vol. 18, Article ID 103024, 2016.

[19] S.-G. Cheng, R.-Z. Zhang, J. Zhou, H. Jiang, and Q.-F. Sun, "Perfect valley filter based on a topological phase in a disordered Sb monolayer heterostructure," *Physical Review B*, vol. 97, no. 8, Article ID 085420, 2018.

[20] X.-T. An, J. Xiao, M. W.-Y. Tu, H. Yu, V. I. Fal'ko, and W. Yao, "Realization of valley and spin pumps by scattering at nonmagnetic disorders," *Physical Review Letters*, vol. 118, no. 9, Article ID 096602, 2017.

[21] V. Hung-Nguyen, S. Dechamps, P. Dollfus, and J.-C. Charlier, "Valley filtering and electronic optics using polycrystalline graphene," *Physical Review Letters*, vol. 117, no. 24, Article ID 247702, 2016.

[22] M. Ezawa, "Valley-polarized metals and quantum anomalous hall effect in silicene," *Physical Review Letters*, vol. 109, no. 5, Article ID 055502, 2012.

[23] M. Li, Z.-L. Cai, Z.-B. Feng, and Z.-Y. Zhao, "Valley-resolved transport in zigzag graphene nanoribbon junctions," *Communications in Theoretical Physics*, vol. 73, no. 11, Article ID 115701, 2021.

[24] S. Hong, Y. Yoon, and J. Guo, "Metal-semiconductor junction of graphene nanoribbons," *Applied Physics Letters*, vol. 92, no. 8, Article ID 083107, 2008.

[25] T. C. Li and S.-P. Lu, "Quantum conductance of graphene nanoribbons with edge defects," *Physical Review B*, vol. 77, no. 8, Article ID 085408, 2008.

[26] Z. Xu, Q.-S. Zheng, and G. Chen, "Elementary building blocks of graphene–nanoribbon-based electronic devices," *Applied Physics Letters*, vol. 90, no. 22, Article ID 223115, 2007.

[27] Y. Wu and P. A. Childs, "Conductance of graphene nanoribbon junctions and the tight binding model," *Nanoscale Research Letters*, vol. 6, Article ID 62, 2011.

[28] L. Ming, H. Hongpei, Z.-B. Feng, and Z. Zhengyin, "Conductance of armchair silicene nanoribbon junctions," *Physica E: Low-Dimensional Systems and Nanostructures*, vol. 111, pp. 172–178, 2019.

[29] J. R. Williams, L. Dicarlo, and C. M. Marcus, "Quantum hall effect in a gate-controlled *p–n* junction of graphene," *Science*, vol. 317, no. 5838, pp. 638–641, 2007.

[30] A. F. Young and P. Kim, "Quantum interference and Klein tunnelling in graphene heterojunctions," *Nature Physics*, vol. 5, pp. 222–226, 2009.

[31] H.-H. Fu, J.-H. Gao, and K.-L. Yao, "Topological field-effect quantum transistors in HgTe nanoribbons," *Nanotechnology*, vol. 25, no. 22, Article ID 225201, 2014.

[32] N. Pournaghavi, M. Esmaeilzadeh, A. Abrishamifar, and S. Ahmadi, "Extrinsic Rashba spin–orbit coupling effect on silicene spin polarized field effect transistors," *Journal of Physics: Condensed Matter*, vol. 29, no. 14, Article ID 145501, 2017.

[33] B. Rzeszotarski and B. Szafran, "Electron spin inversion in gated silicene nanoribbons," *Physical Review B*, vol. 98, no. 7, Article ID 075417, 2018.

[34] H. Tian, C. D. Ren, B. Zhou et al., "Controllable valley polarization using silicene double line defects due to rashba spin–orbit coupling," *Nanoscale Research Letters*, vol. 14, Article ID 350, 2019.

[35] L. Wang, "Thermopower and thermoconductance properties of zigzag edged graphene nanoribbon based thermoelectric module," *Physics Letters A*, vol. 377, no. 21-22, pp. 1486–1490, 2013.

[36] D. N. Sheng, L. Sheng, and Z. Y. Weng, "Quantum hall effect in graphene: disorder effect and phase diagram," *Physical Review B*, vol. 73, no. 23, Article ID 233406, 2006.

[37] Z. Qiao and J. Wang, "A variant transfer matrix method suitable for transport through multi-probe systems," *Nanotechnology*, vol. 18, no. 43, Article ID 435402, 2007.

[38] J. Li and S.-Q. Shen, "Disorder effects in the quantum Hall effect of graphene $p-n$ junctions," *Physical Review B*, vol. 78, no. 20, Article ID 205308, 2008.

[39] C. W. J. Beenakker, "*Colloquium*: Andreev reflection and Klein tunneling in graphene," *Reviews of Modern Physics*, vol. 80, no. 4, pp. 1337–1354, 2008.

[40] S. Datta, *Electronic Transport in Mesoscopic Systems*, Cambridge University Press, Cambridge, England, 1995.

[41] Y.-T. Zhang, F. Zhai, Z. Qiao, and Q.-F. Sun, "Spin-polarized edge modes and snake states in HgTe/CdTe quantum wells under an antisymmetric magnetic field," *Physical Review B*, vol. 86, no. 12, Article ID 121403, 2012.

[42] X.-T. An, Y.-Y. Zhang, J.-J. Liu, and S.-S. Li, "Spin–polarized current induced by a local exchange field in a silicene nanoribbon," *New Journal of Physics*, vol. 14, Article ID 083039, 2012.

[43] W. Ren, Z. Qiao, J. Wang, Q. Sun, and H. Guo, "Universal spin-hall conductance fluctuations in two dimensions," *Physical Review Letters*, vol. 97, no. 6, Article ID 066603, 2006.

[44] D. H. Lee and J. D. Joannopoulos, "Simple scheme for surface-band calculations. II. The green's function," *Physical Review B*, vol. 23, no. 10, pp. 4997–5004, 1981.

[45] M. P. Lopez-Sancho, J. M. Lopez-Sancho, J. M. L. Sancho, and J. Rubio, "Highly convergent schemes for the calculation of bulk and surface Green functions," *Journal of Physics F: Metal Physics*, vol. 15, no. 4, Article ID 851, 1985.

[46] B. Zhou, B. Zhou, X. Chen, W. Liao, and G. Zhou, "Symmetry-dependent spin-charge transport and thermopower through a ZSiNR-based FM/normal/FM junction," *Journal of Physics: Condensed Matter*, vol. 27, no. 46, Article ID 465301, 2015.

[47] B. Zhou, B. Zhou, Y. Yao, G. Zhou, and M. Hu, "Spin-dependent Seebeck effects in a graphene superlattice *p–n* junction with different shapes," *Journal of Physics: Condensed Matter*, vol. 29, Article ID 405303, 2017.

[48] M. Li, Z.-B. Feng, and Z.-Y. Zhao, "Symmetry and magnetization effect on the selective spin–valley polarized transport through the ferromagnetic-normal-ferromagnetic ZSiNR junction," *Physica E: Low-Dimensional Systems and Nanostructures*, vol. 151, Article ID 115729, 2023.